Pathogenic roles and therapeutic potential of the CCL8–CCR8 axis in a murine model of IgG4-related sialadenitis

Fumika Honda
University of Tsukuba Faculty of Medicine: Tsukuba Daigaku Igaku Iryokei https://orcid.org/0000-0002-0762-142X

Hiroto Tsuboi (Hiroto-Tsuboi@md.tsukuba.ac.jp)
University of Tsukuba Faculty of Medicine: Tsukuba Daigaku Igaku Iryokei https://orcid.org/0000-0001-9067-0961

Yuko Ono
University of Tsukuba Faculty of Medicine: Tsukuba Daigaku Igaku Iryokei

Saori Abe
University of Tsukuba Faculty of Medicine: Tsukuba Daigaku Igaku Iryokei

Hiroyuki Takahashi
University of Tsukuba Faculty of Medicine: Tsukuba Daigaku Igaku Iryokei

Kiyoaki Ito
Kanazawa University Graduate School of Medical Sciences: Kanazawa Daigaku Daigakuin Iyaku Hokengaku Sogo Kenkyuka Iyaku Hoken Gakuiki Igakurui

Kazunori Yamada
Kanazawa University Graduate School of Medical Sciences: Kanazawa Daigaku Daigakuin Iyaku Hokengaku Sogo Kenkyuka Iyaku Hoken Gakuiki Igakurui

Mitsuhiro Kawano
Kanazawa University Graduate School of Medical Sciences: Kanazawa Daigaku Daigakuin Iyaku Hokengaku Sogo Kenkyuka Iyaku Hoken Gakuiki Igakurui

Yuya Kondo
University of Tsukuba Faculty of Medicine: Tsukuba Daigaku Igaku Iryokei

Kenichi Asano
Tokyo University of Pharmacy and Life Science: Tokyo Yakka Daigaku

Masato Tanaka
Tokyo University of Pharmacy and Life Science: Tokyo Yakka Daigaku

Marie Malissen
Aix-Marseille Université: Aix-Marseille Universite

Bernard Malissen
Aix-Marseille Université: Aix-Marseille Universite

Isao Matsumoto
University of Tsukuba Faculty of Medicine: Tsukuba Daigaku Igaku Iryokei
Takayuki Sumida
University of Tsukuba Faculty of Medicine: Tsukuba Daigaku Igaku Iryokei

Research article

Keywords: IgG4-related disease, animal model, chemokine, CCL18, CCL8, fibrosis

Posted Date: April 21st, 2021

DOI: https://doi.org/10.21203/rs.3.rs-411178/v1

Version of Record: A version of this preprint was published at Arthritis Research & Therapy on August 14th, 2021. See the published version at https://doi.org/10.1186/s13075-021-02597-6.

Abstract

Background Our previous studies reveal that CCL18-CCR8 chemokine axis is upregulated in patients of immunoglobulin G4-related disease (IgG4-RD), suggest that the CCL18–CCR8 axis is implicated in the etiology of IgG4-RD. Although, whether this axis has a potential as a therapeutic target remains unclear. Our purpose was to clarify the pathogenic roles and therapeutic potential of the murine CCL8 (analogue of human CCL18)–CCR8 axis by using an animal model of IgG4-RD (LAT Y136F knockin mice; LAT mice).

Methods We compared the infiltration of inflammatory cells and the fibrosis of the salivary glands of 6-week-old LAT mice and littermate mice. The expressions of *Ccl8* and *Ccr8* were also compared. Next, we investigated the therapeutic effects of intravenous administration of anti-CCL8 neutralizing antibody in LAT mice against inflammation and fibrosis of the salivary glands. We also investigated the effects of stimulation with recombinant mouse CCL8 on the collagen production in a mouse fibroblast cell line (NIH/3T3) *in vitro.*

Results When compared with the littermates, the LAT mice showed apparent infiltration of inflammatory cells, and fibrosis in the salivary glands. The focus and fibrosis score in the salivary glands were significantly higher in the LAT mice than in the littermates. The expression levels of *Ccl8* in the spleen and of *Ccr8* in the salivary glands were significantly higher in the LAT mice than in the littermates. Anti-CCL8 antibody significantly improved the focus and fibrosis score in the salivary glands of the LAT mice. *In vitro*, stimulation with recombinant mouse CCL8 significantly increased the expression of collagen and ERK1/2 phosphorylation in NIH/3T3.

Conclusion We clarified the overexpression and therapeutic potential of the mouse CCL8–CCR8 axis in LAT mice, which could play a crucial role in fibrosis via ERK1/2 phosphorylation, as well as the chemotaxis of inflammatory cells. The human CCL18–CCR8 axis might be a novel therapeutic target for IgG4-RD.

Background

Immunoglobulin G4-related disease (IgG4-RD) is characterized by elevation of serum IgG4 levels and infiltration of IgG4-positive plasmacytes and fibrosis of multiple organs[1, 2]. Especially in IgG4-RD sialadenitis, the cytokine environment of the salivary glands (SGs) is predominantly composed of type-2 T-helper (Th2) cytokines and IL-10 expression is elevated when compared with the cytokine environment of Sjögren's syndrome, which also presents with sialadenitis (3). In clinical practice, glucocorticoid treatment is effective for inducing clinical remission, but relapse occurs frequently with tapering of the steroid dose[4]. Therefore, a disease-specific treatment strategy based on the etiology is required.

In our previous studies, we revealed that the chemokine (C-C motif) ligand 18 (CCL18) and its receptor chemokine (C-C motif) receptor 8 (CCR8) in labial salivary glands (LSGs) of IgG4-RD patients are upregulated when compared with those of healthy controls and of Sjögren's syndrome patients[5].

Human CCL18 (hCCL18) is produced mainly by macrophages and dendritic cells. It has a chemotactic function for T cells and B cells and induces the fibrosis[6, 7]. We also reported that in the LSGs of IgG4-RD patients, some macrophages and dendritic cells expressed hCCL18[8]. In addition, the number of hCCL18-positive macrophages and dendritic cells in the LSGs of IgG4-RD patients was higher than in those of healthy controls and Sjögren's syndrome patients[8]. Furthermore, hCCL18 specifically enhanced IgG4 production by stimulating peripheral blood mononuclear cells *in vitro*[8]. It was reported that serum hCCL18 concentration was correlated with disease activity and the number of involved organs[9]. These findings suggest that the hCCL18–CCR8 axis is implicated in the etiology of IgG4-RD, although whether this axis has a potential as a therapeutic target remains unclear.

Animal models of disease are essential for the development of therapeutic agents, especially in rare diseases of unknown etiology. However, rodents do not possess the IgG4 subtype, making it difficult to replicate IgG4-RD in a mouse model. The linker for activation of T cells (LAT) Y136F knockin mouse (LAT mouse) has been reported as a mouse with elevated type-2 T-helper (Th2) cytokine and serum IgG1 (human IgG4-equivalent) levels[10]. In recent years, some reports showed that the LAT mouse could be an animal model of IgG4-RD[11, 12]. LAT mice showed IgG1-positive plasmacyte infiltration and fibrosis in some organs, including the SGs, as well as elevated Th2 cytokine and serum IgG1[11]. These characteristics are held in common by human IgG4-RD patients. Furthermore, the tissue lesions of LAT mice were reduced by therapeutic administration of corticosteroid, also in common with human IgG4-RD[11]. Interestingly, it has been reported that CCR8, which is a receptor for hCCL18 and murine CCL8 (mCCL8; analogue of hCCL18), could be upregulated in T cells in a Th2-polarized environment[13] and that IL-4 and IL-10 could induce the production of hCCL18 and mCCL8 from macrophages[13].

In this study, we analyzed the expression levels of the mCCL8 (analogue of hCCL18)–CCR8 axis in LAT mice as a murine model of IgG4-RD and injected the mice with anti-mCCL8 antibody to explore whether mCCL8-blocking therapy would reduce the development of tissue lesions, especially in sialadenitis, in which the elevated expression of hCCL18 has already been demonstrated in human IgG4-RD.

Materials And Methods

Animals

LAT Y136F knockin mice with a C57BL/6j background were kindly provided by Dr Malissen (Marseille Université, Marseille, France) and maintained under specific pathogen-free conditions. All the animal protocols were approved by the Institutional Animal Experiment Committee of the University of Tsukuba (Permit No.20–189), and all the experiments were performed in accordance with relevant guidelines and regulations.

Cell culture and treatment

The NIH/3T3 mouse fibroblast cell line was purchased from the Cell Engineering Division of the RIKEN BioResource Center (Tsukuba, Ibaraki, Japan). The cells were cultured in Dulbecco's modified Eagle's

medium (DMEM) containing antibiotics and 10% fetal bovine serum (FBS) at 37℃ in a humidified incubator containing 5% CO_2. For all the experiments, the cells were used within 3 to 7 passages after the reception. For *in vitro* functional analysis of CCL8, NIH/3T3 cells were seeded in a 96-well plate at a density of 1×10^5 cells/mL. Some groups of cells were cultured with varying concentrations of recombinant mouse CCL8 (BioLegend, San Diego, CA) for 24 h. The concentration of FBS was reduced to 1% at 24 h before testing. Total collagen was detected by the Sirius Red Collagen Detection Kit (Chondrex, Woodinville, WA) according to the manufacturer's instructions.

Histopathologic analysis

The SGs were surgically excised, fixed in neutralized 10% formalin, and embedded in paraffin, and 3-μm-thick slices were prepared. The slices were stained with hematoxylin and eosin (H&E) and with Masson's trichrome (M&T) according to the standard techniques. The inflammatory lesions were graded histologically using the focus score method proposed by Greenspan et al[14] as follows: the focus score was described as the number of a focus per 4 mm^2 of each section. One focus was defined as > 50 mononuclear cells found around the SG ducts. The fibrotic lesions were graded as occupancy of fibrosis per 4 mm^2 of each section: 0: without fibrosis; 1: 1 to 24%; 2: 25 to 49%; 3: higher than 50%. The histopathologic evaluation was performed by means of light microscopy in a blinded manner.

Immunofluorescence and immunohistochemical staining

For confocal microscopy, the organs were embedded in optimum cutting temperature (OCT) compound (Tissue-Tek; Sakura Finetek, Tokyo, Japan) and frozen at -80℃. A cryostat was used to generate 5-μm slices, which were kept at -20℃. On the day of staining, the slices were thawed and dried and then fixed with cold acetone for 10 min. The slices were rehydrated in phosphate-buffered saline (PBS), blocked in PBS containing 1% bovine serum albumin (BSA; FujiFilm Wako Pure Chemical, Tokyo, Japan) for 30 min at 20℃–22℃, and stained with Alexa Fluor 488-conjugated rat anti-mouse CD4 antibody (Thermo Fisher Scientific, Waltham, MA) or with Alexa Fluor 647-conjugated rat anti-mouse B220, Alexa Fluor 488-conjugated rat anti-mouse F4/80 antibody, and Alexa Fluor 488-conjugated rat anti-mouse CD11c antibody (all from BioLegend). For double staining of CCL8 and cell surface molecules, the slices were blocked in 3% H_2O_2 in methanol to block endogenous biotin, and stained with biotinylated anti-mouse MCP-2/CCL8 antibody (R&D Systems, Minneapolis, NE). The primary antibody was left to incubate overnight at 4℃. Streptavidin-Alexa Fluor 594 (BioLegend) was used as a secondary antibody and was left to incubate for 30 min at 20℃–22℃. For staining of CCR8, the cells were applied to glass slides by use of Smear Gel (GenoStaff, Tokyo, Japan) according to the manufacturer's instructions. After being blocked in PBS containing 1% BSA, the slices were stained with anti-mouse CCR8 antibody (Abcam, Cambridge, UK) and incubated overnight at 4℃. Alexa Fluor 546 goat anti-rabbit IgG (H + L) (Thermo Fisher Scientific) was used as a secondary antibody. The control slides were incubated with a dilution buffer containing isotype-matched antibodies instead of primary antibodies. All the dilutions were made in Solution B (Toyobo, Osaka, Japan). The nuclei were counterstained with 4',6-diamidino-2-phenylindole (DAPI). All the slides were mounted in Fluorescence Mounting Medium (Dako Carpinteria, Santa Barbara, CA). For immunohistochemical staining, 5-μm slices were cut from formalin-fixed and paraffin-embedded

tissues, deparaffinized, rehydrated, blocked in PBS containing 1% BSA for 30 min at 20℃–22℃, and then stained with anti-mouse CD138 antibody (BioLegend). After incubation overnight at 4℃, the slices were washed in PBS 5 times and incubated with Histofine Simple Stain MAX-PO (Nichirei Bio, Tokyo, Japan) for 30 min at 20℃–22℃. Peroxidase activity was detected with diaminobenzidine (Nichirei Bio). The slices were counterstained with hematoxylin and dehydrated. A Fluoview FV10i confocal laser scanning microscope (Olympus, Tokyo, Japan) or Biozero BZ-8100 (Keyence, Osaka, Japan) was used to acquire images.

RNA extraction and quantitative real-time reverse-transcription polymerase chain reaction (qRT-PCR)

Cervical lymph nodes (cLNs) and SGs were submerged in approximately 5 volumes of RNAlater solution (Thermo Fisher Scientific) immediately after sampling. Spleens were strained through a 40-μm filter and subjected to red blood cell (RBC) lysis with 0.16 M of NH_4Cl solution for 5 min. These samples or cultured NIH/3T3 mouse fibroblast cells were suspended in Isogen (Nippon Gene, Tokyo, Japan). Total RNA was extracted using the Isogen method. Complementary DNA (cDNA) was synthesized at 37℃ for 15 min using a Prime Script reverse transcriptase master mix (Takara Bio, Shiga, Japan), and the reaction mixture was used for the PCR. qRT-PCR reactions were performed using a Taqman gene expression assay and normalized to glyceraldehyde-3-phosphate dehydrogenase *(Gapdh)* abundance. The primers and probes, all from Thermo Fisher Scientific, were as follows: *Gapdh*, Mm99999915_g1; *Ccr8*, Mm99999115-s1; *Ccl8*, Mm01297183-m1; *IL4*, Mm00445259_m1; *IL10*, Mm00439614_m1; *Col1a2*, Mm00483888_m1.

Enzyme-linked immunosorbent assay (ELISA)

Serum levels of mouse CCL8 were measured using a commercially available ELISA (R&D systems) according to the manufacturer's instructions.

Fluorescence-activated cell sorting (FACS) staining

For FACS analyses, the cells were washed in FACS buffer (2% FBS in PBS) and then incubated with FACS antibodies. For phosphoextracellular signal-regulated kinase (ERK)1/2 (BioLegend) staining, Phosflow Lyse/Perm buffer and Perm Buffer III (Becton, Dickinson and Company [BD], Franklin Lakes, NJ) were used according to the manufacturer's instructions. The samples were analyzed with a FACSVerse flow cytometer (BD), and the data were analyzed using FlowJo software (Tree Star, Ashland, OR). The relative mean fluorescence intensity (MFI) ratio was calculated on the basis of the ratio of the MFI for a marker to the MFI of its isotype control.

In vivo inhibition of CCL8

One hundred micrograms of anti-mouse CCL8 neutralizing antibody (clone 17D6, generated by the Tokyo University of Pharmacy and Life Sciences, Tokyo) or isotype control (BioLegend) was intravenously injected on days 1 and 2 in 5-week-old LAT mice on the basis of a previous study[15]. On day 8 (6 weeks of age), the effects of treatment on the development of tissue lesions (spleen, cLNs, and SGs) were assessed.

Statistical analysis

All the data were expressed as means ± SEMs. Differences between groups were examined for significance using a 2-tailed unpaired *t* test or Kruskal-Wallis test. Probability values lower than 0.05 were considered to indicate significant differences. Statistical analysis was performed using GraphPad Prism version 9 (GraphPad software, San Diego, CA).

Results

Histopathologic analysis of the salivary glands of 6-week-old LAT mice and littermates

We histopathologically analyzed the SGs of 6-week -old LAT mice and the control littermates. All the analyzed LAT mice displayed inflammatory lesions showing infiltration of mononuclear cells with fibrosis (Fig. 1**[A]**). The histologic focus scores and fibrosis scores of the LAT mice were significantly higher than those of the littermates (Fig. 1**[B][C]**). Immunostaining revealed infiltration of $CD4^+$ T cells, $B220^+$ B cells, and $CD138^+$ plasma cells into the SGs of the LAT mice (Fig. 1**[D][E]**).

Upregulation of the CCL8–CCR8 axis in the salivary glands of LAT mice

To clarify whether Th2 cytokines and the CCL8–CCR8 axis are upregulated in LAT mice as they are in IgG4-RD patients, we compared *Il4*, *Il10, Ccl8, and Ccr8* mRNA expressions in the spleen, cLNs, and SGs of the LAT mice and the littermates. Our results showed that *Il4* expression in the spleen, cLNs, and SGs of the LAT mice was significantly higher than that in the littermates (Fig. 2**[A]**). *Il10* and *Ccl8* expressions were significantly higher in the spleen (Fig. 2**[B][C]**), and *Il10* and *Ccr8* expressions were significantly higher in the SGs of the LAT mice (Fig. 2**[D]**). Besides, serum CCL8 levels were significantly higher in the LAT mice than in the littermates (Fig. 2**[E]**). These data suggested that the LAT mice also had a Th2-dominant cytokine environment similar to IgG4-RD and that the CCL8–CCR8 axis was enhanced.

CCL8-expressing cells in the salivary glands of LAT mice

To confirm that mCCL8-expressing cells were exactly present in the SGs, we immunofluorescently stained the infiltrating cells. The results revealed that CCL8-expressing F4/80-positive macrophages (Fig. 3**[A]**) and CD11c-positive dendritic cells (Fig. 3**[B]**) were predominantly present in the SGs of the LAT mice. In contrast, these cells were not detected in the littermates.

Suppression of salivary gland inflammation and fibrosis in LAT mice by administration of anti-mCCL8 neutralizing antibody

To determine whether the mCCL8-CCR8 pathway could be a therapeutic target for IgG4-RD, we evaluated the SG pathology of anti-mCCL8 neutralizing antibody- (anti-CCL8 Ab) and control immunoglobulin-

(control Ig) treated LAT mice. The development of sialadenitis was found to be inhibited in the anti-CCL8 Ab-treated LAT mice when compared with the control Ig-treated mice (Fig. 4**[A]**). The focus scores of the anti-CCL8 Ab-treated mice were significantly lower than those of the control Ig-treated mice (Fig. 4**[B]**). Interestingly, the development of SG fibrosis was also found to be inhibited in the anti-CCL8 Ab-treated LAT mice (Fig. 4**[C]**). The fibrosis scores of the anti-CCL8 Ab-treated mice were significantly lower than those of the control Ig-treated mice (Fig. 4**[D]**). Immunostaining revealed that the number of $CD4^+$ cells that had infiltrated the region around the SG ducts of the anti-CCL8 Ab-treated mice was significantly reduced when compared with that of the control Ig-treated mice (Fig. 4**[E][F]**). The number of $B220^+$ cells and $CD138^+$ cells also tended to be reduced, although the difference between the treatment groups did not reach statistical significance. (Fig. 4**[E][G][H][I]**).

Effects of CCL8-blocking therapy on mRNA expression of Il4 and Il10 in LAT mice

Next, we investigated whether anti-mCCL8 neutralizing therapy affected the cytokine environment in LAT mice. The mRNA expression of *Il4* and *Il10* tended to be reduced in the anti-CCL8 Ab-treated LAT mice when compared with the control Ig-treated group, especially in the spleen, although the difference between the treatment groups did not reach statistical significance (Fig. 5**[A][B]**). These results could suggest that the attenuated Th2 phenotypes were not the main reason for the improved fibrosis. The following *in vitro* experiment was conducted to investigate the possibility that mCCL8 acts directly on fibroblasts and has a mechanism involved in fibrosis.

Effects of mCCL8 on collagen production of fibroblasts in vitro

To further analyze the association between mCCL8 and fibrosis, we cultured a mouse fibroblast cell line (NIH/3T3) with or without recombinant mouse CCL8 (rmCCL8). First, we confirmed the protein expression of CCR8 in NIH/3T3 cells by means of immunofluorescence staining (Fig. 6**[A]**). Then, the NIH/3T3 cells were stimulated with various concentrations of rmCCL8. Twenty-four hours after the stimulation with rmCCL8, we investigated the mRNA expression level of *Col1a2* and the total collagen protein production in the NIH/3T3 cells. The mRNA expression levels of *Col1a2* and the total collagen protein production were increased in rmCCL8 dose-dependent manner. (Fig. 6**[B][C]**). To investigate whether ERK1/2 phosphorylation is involved in upregulation of collagen production by rmCCL8, the NIH/3T3 cells were treated with 300 ng/mL of rmCCL8. After 12 min of stimulation with rmCCL8, phosphorylation of ERK1/2 in the NIH/3T3 cells was significantly increased in both the MFI and the positive cell ratio when compared with no stimulation (Fig. 6**[D][E][F]**). Thus, our data suggested that the mCCL8-CCR8 pathway is involved in the induction of collagen production by fibroblasts via phosphorylation of ERK1/2.

Discussion

In this study, we showed that LAT mice had plasmacyte infiltration and fibrosis of the SGs similar to human IgG4-RD as well as an enhanced CCL8–CCR8 axis. Neutralization of mCCL8 showed

improvement of sialadenitis including fibrosis, and it was shown that mCCL8 may enhance collagen production in fibroblasts via phosphorylation of ERK1/2. Through our investigation, the following 3 clinicopathologic findings emerged.

First, commonalities between LAT mice and IgG4-RD have been further demonstrated. The expression levels of the mCCL8–CCR8 axis were upregulated in LAT mice, in common with those of hCCL18–CCR8 in IgG4-RD. Therefore, we thought that the potential of the mCCL8 (hCCL18)–CCR8 pathway as a therapeutic target could be clarified by using LAT mice as a model of IgG4-RD. The chemokine–chemokine receptor system in mice differs from that in humans[6]. In mice, CCL1 and CCL8 have been reported as a ligands for CCR8[13]. The relationship between hCCL18 and mCCL8, not mCCL1, has been proven to be a functional analogue[16]. Focusing on the induction mechanism, IL-4 and IL-10 induce mCCL8 production from macrophages, and the same can be said for hCCL18[13]. In LAT mice, infiltration of mCCL8-producing macrophages was observed in the SGs. Furthermore, both *Il4* and *Il10* were highly expressed in the SGs of LAT mice, and this environment may induce mCCL8 production.

Second, our results suggest that the CCL8–CCR8 axis may have a potential as a therapeutic target for IgG4-RD. The improvement of inflammatory cell infiltration was thought to be due to the suppression of chemotaxis of T cells and B cells to the SGs in which mCCL8 was produced by macrophages and dendritic cells. Expression of CCR8 in T cells was reportedly upregulated in the Th2 cytokine environment[13]. Since LAT mice showed a Th2 cytokine-dominant phenotype, like that of IgG4-RD[10], it is an environment in which CCR8 expression in T cells is likely to be enhanced. Even more interesting, anti-CCL8 Ab improved not only the infiltration of inflammatory cells but also the fibrosis of the SGs. Thus, the CCL8–CCR8 axis may have pathogenic roles beyond the chemotaxis of lymphocytes, such as induction of fibrosis.

Third, we showed for the first time that mCCL8 could induce collagen production in fibroblasts via ERK1/2 phosphorylation. Although many unclear points about the downstream pathway of CCR8 remained, it was reported that ERK phosphorylation occurred when a signal from the ligand was input in this pathway[17, 18]. ERK was contained in mitogen-activated protein kinase (MAPK)[19], which transmitted extracellular stimuli into cells, and ERK1/2 has been reported to induce fibroblast proliferation[20]. Still only a limited amount of evidence is available related to the function of hCCL18 in inducing collagen production in fibroblasts[7], and it was reported that the Th2 cytokine environment itself was involved in the induction of fibrosis[21]. Importantly, our data suggest that mCCL8 could induce collagen production in fibroblasts via an ERK-dependent pathway, independently of Th2 cytokines.

The following has been reported regarding the fibrotic mechanism in human IgG4-RD. $CD4^+$ T cells with cytotoxic activity ($CD4^+$CTL), which were clonally proliferated in the affected organs, expressed cytotoxic proteins such as granzyme B and perforin[22]. These cells produce IL-1β, IFNγ, and TGFβ, which activates fibroblasts and alternatively activated (M2) macrophages, thereby inducing fibrosis in IgG4-related dacryoadenitis and sialadenitis[23]. Moreover, the number of infiltrating M2 macrophages has been reported to correlate with the fibrosis score in IgG4-related sialadenitis and that these macrophages

produce hCCL18[24]. These reports also supposed that hCCL18 acted as a profibrotic factor and that the hCCL18–CCR8 axis may be a therapeutic target for IgG4-RD.

The role of chemokines in directing T-cell polarization in addition to their role in chemoattraction has been shown in several reports; for example, CXCL10 for T-helper type-1 cells[25, 26], CXCL11 and CXCL12 for T regulatory-1 cells[27, 28], and CCL1 for $FOXp3^+$ Treg cells[17] have been reported to be involved in the polarization and differentiation of $CD4^+$ T cells. Analysis of the effect of the mCCL8 (hCCL18)–CCR8 axis on CD4-positive T-cell differentiation needs to be further investigated. Moreover, we hope that our research findings to lead to the development of treatments targeting the hCCL18–CCR8 pathway as a rescue therapy for intractable IgG4-RD cases such as steroid-resistant cases and recurrent cases.

Conclusions

In conclusion, we have demonstrated that upregulation of the mCCL8 (analogue of hCCL18)–CCR8 axis in LAT mice could play a crucial role in fibrosis via ERK1/2 pathway-dependent type-I collagen production, as well as in cell infiltration in sialadenitis. In fact, anti-CCL8 Ab improved both the inflammation and the fibrosis of SGs in LAT mice, suggesting that inhibition of the hCCL18 (mCCL8)–CCR8 axis should shed light on new therapies for IgG4-RD.

List Of Abbreviations

IgG4-RD; Immunoglobulin G4-related disease

LAT; the linker for activation of T cells

LAT mice; LAT Y136F knockin mice

SGs; salivary glands

anti-CCL8 neutralizing antibody; anti-CCL8 Ab

recombinant mouse CCL8; rmCCL8

LSGs; labial salivary glands

mCCL8; murine CCL8

hCCL18; human CCL18

Th2; type-2 T-helper

DMEM; Dulbecco's modified Eagle's medium

FBS; fetal bovine serum

H&E; hematoxylin and eosin

M&T; Masson’s trichrome

PBS; phosphate-buffered saline

qRT-PCR; quantitative real-time reverse-transcription polymerase chain reaction cLNs; cervical lymph nodes

RBC; red blood cell

cDNA; complementary DNA

Gapdh; glyceraldehyde-3-phosphate dehydrogenase

ELISA; enzyme-linked immunosorbent assay

FACS; Fluorescence-activated cell sorting

ERK; extracellular signal-regulated kinase

MFI; mean fluorescent intensity

control Ig; control immunoglobulin

MAPK; mitogen-activated protein kinase

$CD4^+$CTL; $CD4^+$ T cells with cytotoxic activity

Declarations

Acknowledgements

We thank Dr. F Miyamasu, Medical English Communication Center, University of Tsukuba, for critical reading of the manuscript.

Funding

This work was supported in part by a grant from the Practical Research Project for Rare/Intractable Diseases (IgG4-related disease) of the Japan Agency for Medical Research and Development (AMED).

Authors’ contributions

FH; conceptualization, investigation, formal analysis, visualization and writing the original draft. H Tsuboi; conceptualization, supervision, and visualization and writing the original draft. YO; conceptualization, SA; conceptualization, H Takahashi, conceptualization and supervision, KI;

conceptualization and resources, KY; conceptualization and resources, MK; conceptualization and resources, YK; conceptualization and supervision, KA; methodology and resources, MT; methodology and resources, MM; conceptualization and resources, BM; conceptualization and resources, IM; conceptualization and supervision, TS; conceptualization and supervision. All authors contributed to the review and editing of the manuscripts.

Availability of data and materials

The data that support the findings of this study are available from the corresponding author upon reasonable request.

Ethics approval and consent to participate

All the animal protocols were approved by the Institutional Animal Experiment Committee of the University of Tsukuba (Permit No.20-189), and all the experiments were performed in accordance with relevant guidelines and regulations.

Consent for publication

All authors gave their consent to publication of this manuscript.

Competing interests

The authors declare that they have no competing interests.

References

1. Stone JH, Zen Y, Deshpande V. IgG4-Related Disease. N Engl J Med. 2012;366:539–51.
2. Umehara H, Okazaki K, Masaki Y, Kawano M, Yamamoto M, Saeki T, et al. Comprehensive diagnostic criteria for IgG4-related disease (IgG4-RD), 2011. Mod Rheumatol. 2012;22:21–30.
3. Tanaka A, Moriyama M, Nakashima H, Miyake K, Hayashida JN, Maehara T, et al. Th2 and regulatory immune reactions contribute to IgG4 production and the initiation of Mikulicz disease. Arthritis Rheum. 2012;64:254–63.
4. Yamamoto M, Takahashi H, Shinomura Y. Mechanisms and assessment of IgG4-related disease: Lessons for the rheumatologist. Nat Rev Rheumatol. 2014;10:148–59.
5. Tsuboi H, Nakai Y, Iizuka M, Asashima H, Hagiya C, Tsuzuki S, et al. DNA microarray analysis of labial salivary glands in IgG4-related disease: Comparison with Sjögren's syndrome. Arthritis Rheumatol. 2014;66:2892–9.
6. Chenivesse C, Tsicopoulos A. CCL18 – Beyond chemotaxis. Cytokine. 2018;109:52–6.
7. Atamas SP, Luzina IG, Choi J, Tsymbalyuk N, Carbonetti NH, Singh IS, et al. Pulmonary and Activation-Regulated Chemokine Stimulates Collagen Production in Lung Fibroblasts. Am J Respir Cell Mol Biol. 2003;29:743–9.

8. Tsuboi H, Iizuka-Koga M, Asashima H, Takahashi H, Kudo H, Ono Y, et al. Upregulation and pathogenic roles of CCL18-CCR8 axis in IgG4-related disease. Mod Rheumatol. Taylor & Francis; 2020;30:729–37.
9. Akiyama M, Yasuoka H, Yoshimoto K, Takeuchi T. CC-chemokine ligand 18 is a useful biomarker associated with disease activity in IgG4-related disease. Ann Rheum Dis. 2018;77:1386–7.
10. Aguado E, Richelme S, Nuñez-Cruz S, Miazek A, Mura AM, Richelme M, et al. Induction of T helper type 2 immunity by a point mutation in the LAT adaptor. Science. 2002;296:2036–40.
11. Yamada K, Zuka M, Ito K, Mizuguchi K, Kakuchi Y, Onoe T, et al. LatY136F knock-in mouse model for human IgG4-related disease. PLoS One. 2018;13:1–14.
12. Cui Y, Masaki K, Zhang X, Yamasaki R, Fujii T, Ogata H, et al. A novel model for treatment of hypertrophic pachymeningitis. Ann Clin Transl Neurol. 2019;6:431–44.
13. Islam SA, Ling MF, Leung J, Shreffler WG, Luster AD. Identification of human CCR8 as a CCL18 receptor. J Exp Med. 2013;210:1889–98.
14. Greenspan JS, Daniels TE, Talal N, Sylvester RA. The histopathology of Sjögren's syndrome in labial salivary gland biopsies. Oral Surgery. Oral Med Oral Pathol. 1974;37:217–29.
15. Asano K, Takahashi N, Ushiki M, Monya M, Aihara F, Kuboki E, et al. Intestinal CD169 + macrophages initiate mucosal inflammation by secreting CCL8 that recruits inflammatory monocytes. Nat Commun Nature Publishing Group. 2015;6:1–14.
16. Islam SA, Chang DS, Colvin RA, Byrne MH, McCully ML, Moser B, et al. Mouse CCL8, a CCR8 agonist, promotes atopic dermatitis by recruiting IL-5 + TH2 cells. Nat Immunol. 2011;12:167–77.
17. Barsheshet Y, Wildbaum G, Levy E, Vitenshtein A, Akinseye C, Griggs J, et al. CCR8 + FOXp3 + Treg cells as master drivers of immune regulation. Proc Natl Acad Sci U S A. 2017;114:6086–91.
18. Spinetti G. The chemokine receptor CCR8 mediates rescue from dexamethasone-induced apoptosis via an ERK-dependent pathway. J Leukoc Biol. 2003;73:201–7.
19. Segar R, Krebs EG. The MAPK signaling cascade. FASEB J. 1995;9:726–35.
20. Ihn H, Tamaki K. Oncostatin M. Stimulates the Growth of Dermal Fibroblasts Via a Mitogen-Activated Protein Kinase-Dependent Pathway. J Immunol. 2000;165:2149–55.
21. Jinnin M, Ihn H, Yamane K, Tamaki K. Interleukin-13 stimulates the transcription of the human α2(I) collagen gene in human dermal fibroblasts. J Biol Chem. 2004;279:41783–91.
22. Mattoo H, Mahajan VS, Maehara T, Deshpande V. Clonal expansion of CD4 1 cytotoxic T lymphocytes in patients with IgG 4 -related disease. J Allergy Clin Immunol. 2016;138:825–38.
23. Maehara T, Mattoo H, Ohta M, Mahajan VS, Moriyama M, Yamauchi M, et al. Lesional CD4 + IFN-γ + cytotoxic T lymphocytes in IgG4-related dacryoadenitis and sialoadenitis. Ann Rheum Dis. 2017;76:377–85.
24. Furukawa S, Moriyama M, Tanaka A, Maehara T, Tsuboi H, Iizuka M, et al. Preferential M2 macrophages contribute to fibrosis in IgG4-related dacryoadenitis and sialoadenitis, so-called Mikulicz's disease. Clin Immunol. 2015;156:9–18.

25. Salomon I, Netzer N, Wildbaum G, Schif-Zuck S, Maor G, Karin N. Targeting the Function of IFN-γ-Inducible Protein 10 Suppresses Ongoing Adjuvant Arthritis. J Immunol. 2002;169:2685–93.
26. Wildbaum G, Netzer N, Karin N. Plasmid DNA Encoding IFN-γ-Inducible Protein 10 Redirects Antigen-Specific T Cell Polarization and Suppresses Experimental Autoimmune Encephalomyelitis. J Immunol. 2002;168:5885–92.
27. Zohar Y, Wildbaum G, Novak R, Salzman AL, Thelen M, Alon R, et al. CXCL11-dependent induction of FOXP3-negative regulatory T cells suppresses autoimmune encephalomyelitis. J Clin Invest. 2017;127:3913.
28. Meiron M, Zohar Y, Anunu R, Wildbaum G, Karin N. CXCL12 (SDF-1α) suppresses ongoing experimental autoimmune encephalomyelitis by selecting antigen-specific regulatory T cells. J Exp Med. 2008;205:2643–55.

Figures

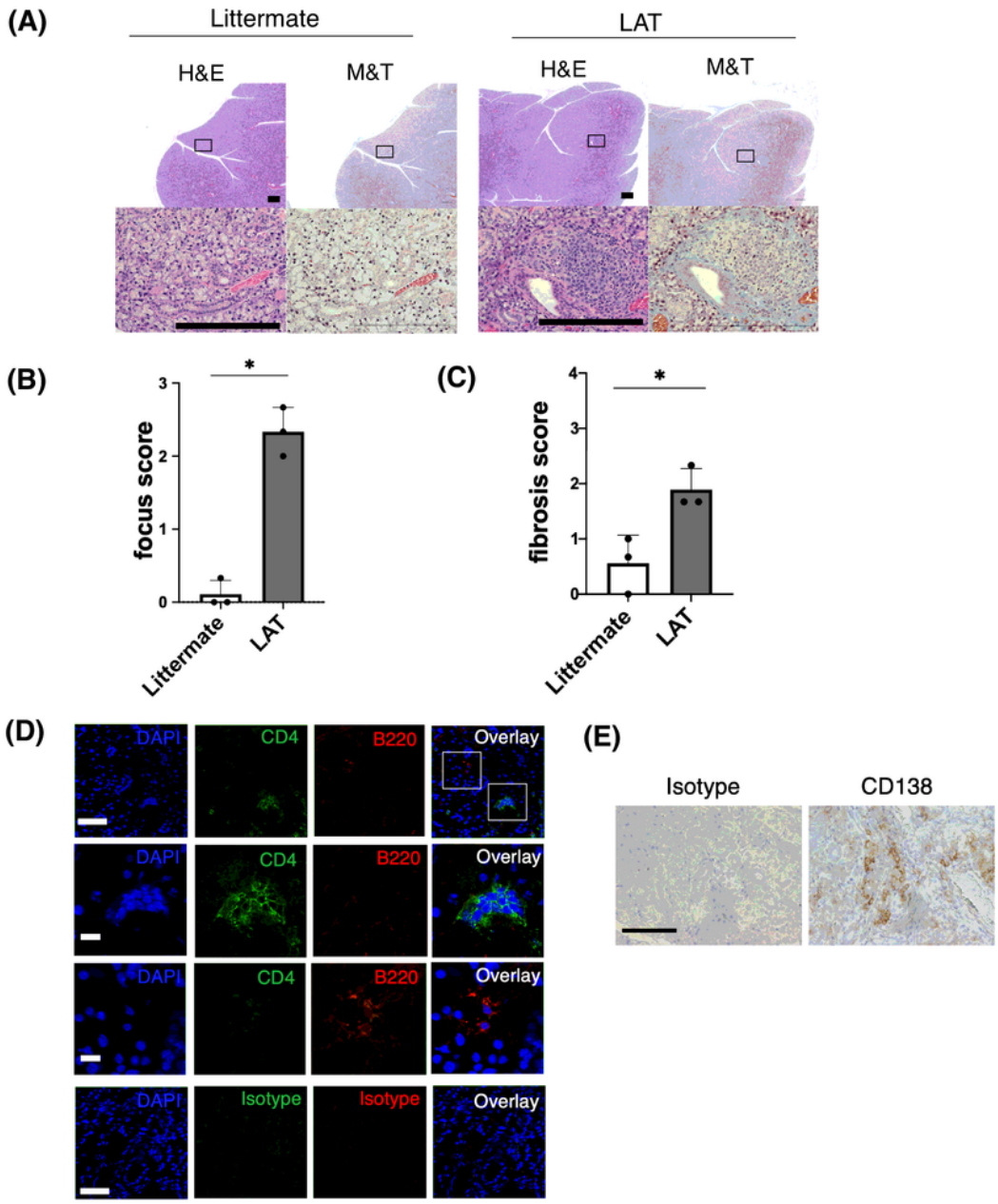

Figure 1

Histologic analysis of the salivary glands of 6-week-old LAT mice and of the littermates (A) H&E staining and M&T staining of salivary glands. The boxed areas in the upper panels are shown in detail in the lower panels. Scale bars, 200 μm. Representative images of 3 mice per group. H&E, hematoxylin and eosin stain; M&T, Masson's trichrome stain. (B) Focus score of salivary glands. Histologic evaluation was performed in a blinded manner. (littermate, n = 3; LAT mice, n = 3). (C) Fibrosis score of salivary glands.

Histologic evaluation was performed in a blinded manner. (littermate, n = 3; LAT mice, n = 3). (D) Images are representative of salivary gland slices of LAT mice stained for CD4 (green), B220 (red), and 4'6-diamino-2-phenylindole (DAPI) (blue). Top: low magnification images; second row from the top: the part focused on CD4+ cells; third row from the top: the part focused on B220+ cells; bottom row: images stained for isotype control. Scale bars (top, 50 μm; second and third rows from the top, 10 μm; bottom row, 50 μm). (E) Salivary gland slices of LAT mice stained for CD138 or isotype control. Scale bar,100 μm. *p<0.05, Unpaired t test.

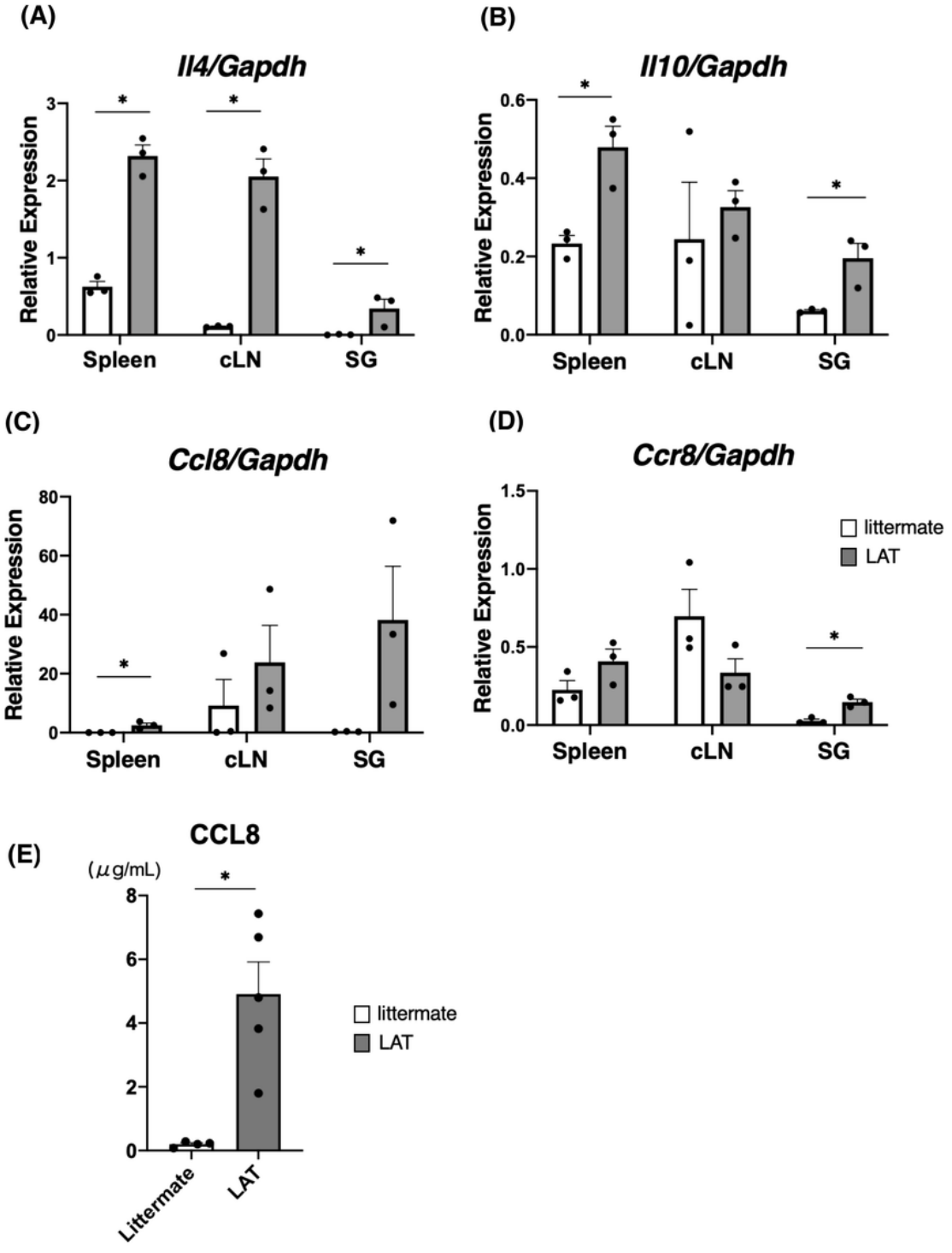

Figure 2

Upregulation of Th2 cytokines and the CCL8–CCR8 axis in 6-week-old LAT mice (A) Il4 mRNA levels in spleens, cervical lymph nodes (cLNs), and salivary glands (SGs) were determined by qRT-PCR. The expression levels were calculated as relative amounts normalized to Gapdh. (littermate, n = 3; LAT, n = 3). (B) Il10 mRNA levels in spleens, cLNs, and SGs were determined by qRT-PCR. The expression levels were calculated as relative amounts normalized to Gapdh. (littermate, n = 3; LAT, n = 3). (C) Ccl8 mRNA levels in each tissue were determined by means of qRT-PCR. The expression levels were calculated as relative amounts normalized to Gapdh. (littermate, n = 3; LAT, n = 3). (D) Ccr8 mRNA levels in each tissue was determined by means of qRT-PCR. The expression levels were calculated as relative amounts normalized to Gapdh. (littermate, n = 3; LAT, n = 3). (E) Serum CCL8 levels were determined by ELISA. (littermate, n = 4; LAT, n = 5). *$p<0.05$, Unpaired t test. The data are presented as means ± SEMs.

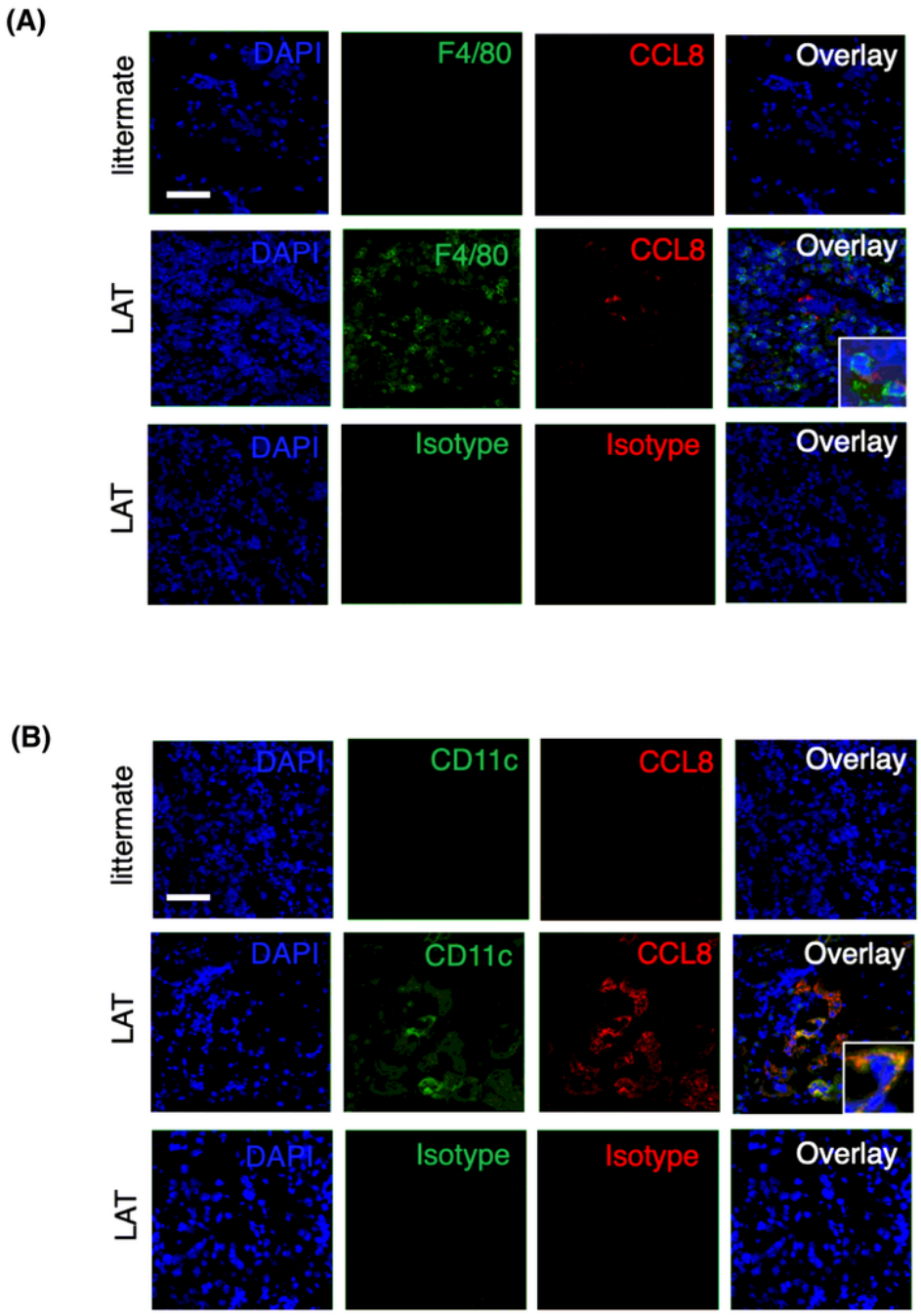

Figure 3

CCL8-expressing cells in salivary glands of LAT mice (A) Salivary gland slices from 6-week-old control littermates or LAT mice were stained for F4/80 (green) and CCL8 (red). (B) Salivary gland slices from 6-week-old control littermates or LAT mice were stained for CD11c (green) and CCL8 (red). DAPI (blue), 4'6-diamino-2-phenylindole. Scale bars, 50 μm.

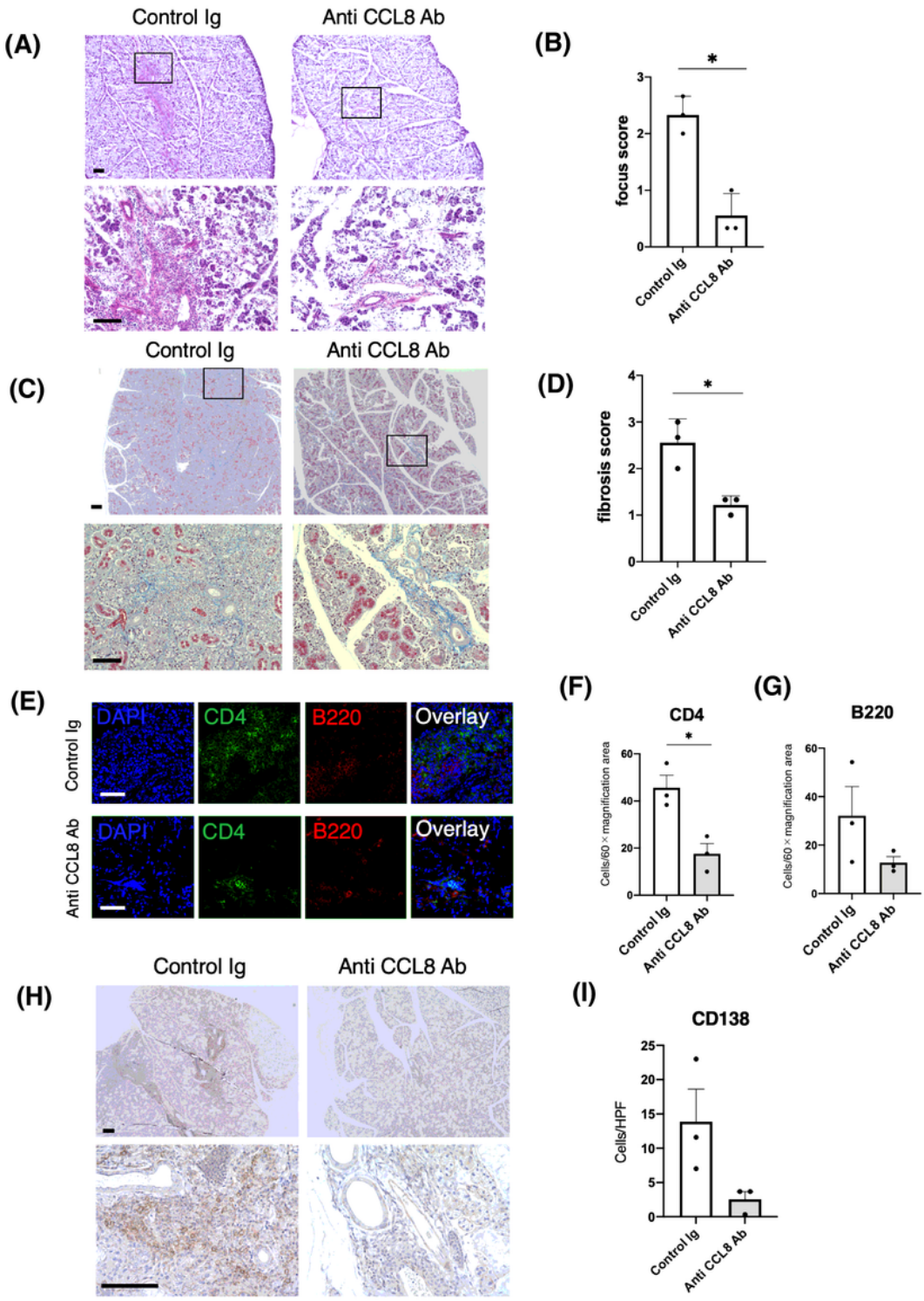

Figure 4

Suppression of salivary gland inflammation and fibrosis in LAT mice by CCL8 neutralizing therapy (A) H&E staining of salivary glands in LAT mice treated with anti-CCL8 neutralizing antibody (anti-CCL8 Ab) or control immunoglobulin (control Ig). The boxed areas in the upper panels are shown magnified in the lower panels. (Scale bars: upper; 200 μm; lower, 100 μm). Representative images of 3 mice. (B) Comparison of focus score in salivary glands between anti-CCL8 Ab-treated LAT mice and control Ig-

treated LAT mice. (C) M&T staining of salivary glands in LAT mice treated with anti-CCL8 Ab or control Ig. The boxed areas in the upper panels are magnified in the lower panels. (Scale bars: upper, 200 μm; lower, 100 μm). Representative images of 3 mice. (D) Comparison of fibrosis score in salivary glands of anti-CCL8 Ab-treated LAT mice and control Ig-treated LAT mice. (E) The salivary glands slices of LAT mice treated with anti-CCL8 Ab or control Ig were stained for CD4 (green) and B220 (red). DAPI (blue), 4'6-diamino-2-phenylindole. (Scale bars, 50 μm). (F) The average of CD4-positive cells per 60× magnification area. Three areas per mouse were counted. (G) The average of B220-positive cells per 60× magnification area. Three areas per mouse were counted. (H) Salivary glands slices of LAT mice treated with anti-CCL8 Ab or control Ig were stained for CD138. Counterstaining was done with hematoxylin. (Scale bars: upper, 200 μm; lower, 100 μm). (I) The average of CD138-positive cells per high power field. Three areas per mouse were counted. The data are presented as the means ± SEMs of 3 mice. *$p<0.05$, Unpaired t test.

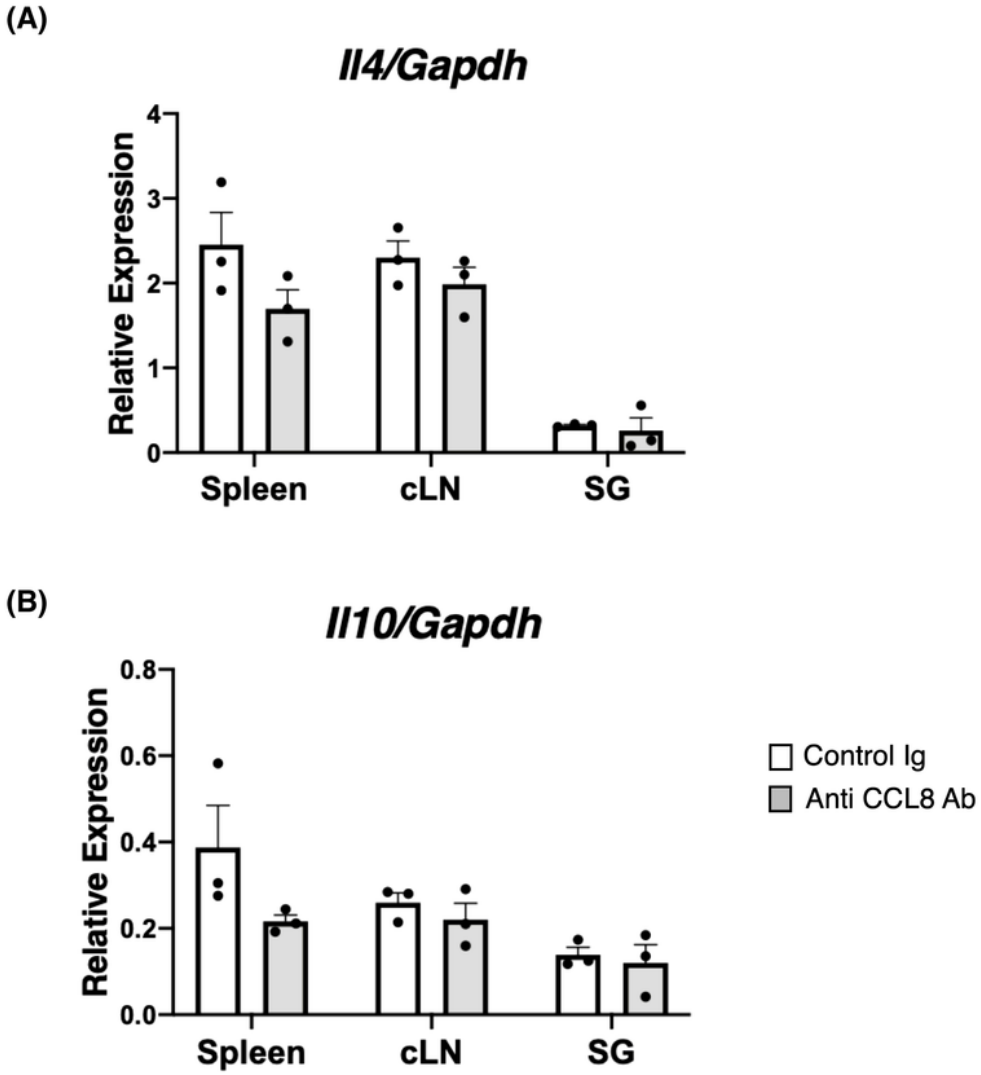

Figure 5

Effects of CCL8-blocking therapy on mRNA expression of Il4 and Il10 in LAT mice (A) Comparison of mRNA expression levels of Il4 in anti-CCL8 Ab-treated LAT mice and control Ig-treated LAT mice. (B) Comparison of mRNA expression levels of Il10 in anti-CCL8 Ab-treated LAT mice and control Ig-treated LAT mice. cLN, cervical lymph nodes; SG, salivary glands. The data are presented as means ± SEMs of 3 mice. *p<0.05, unpaired t test.

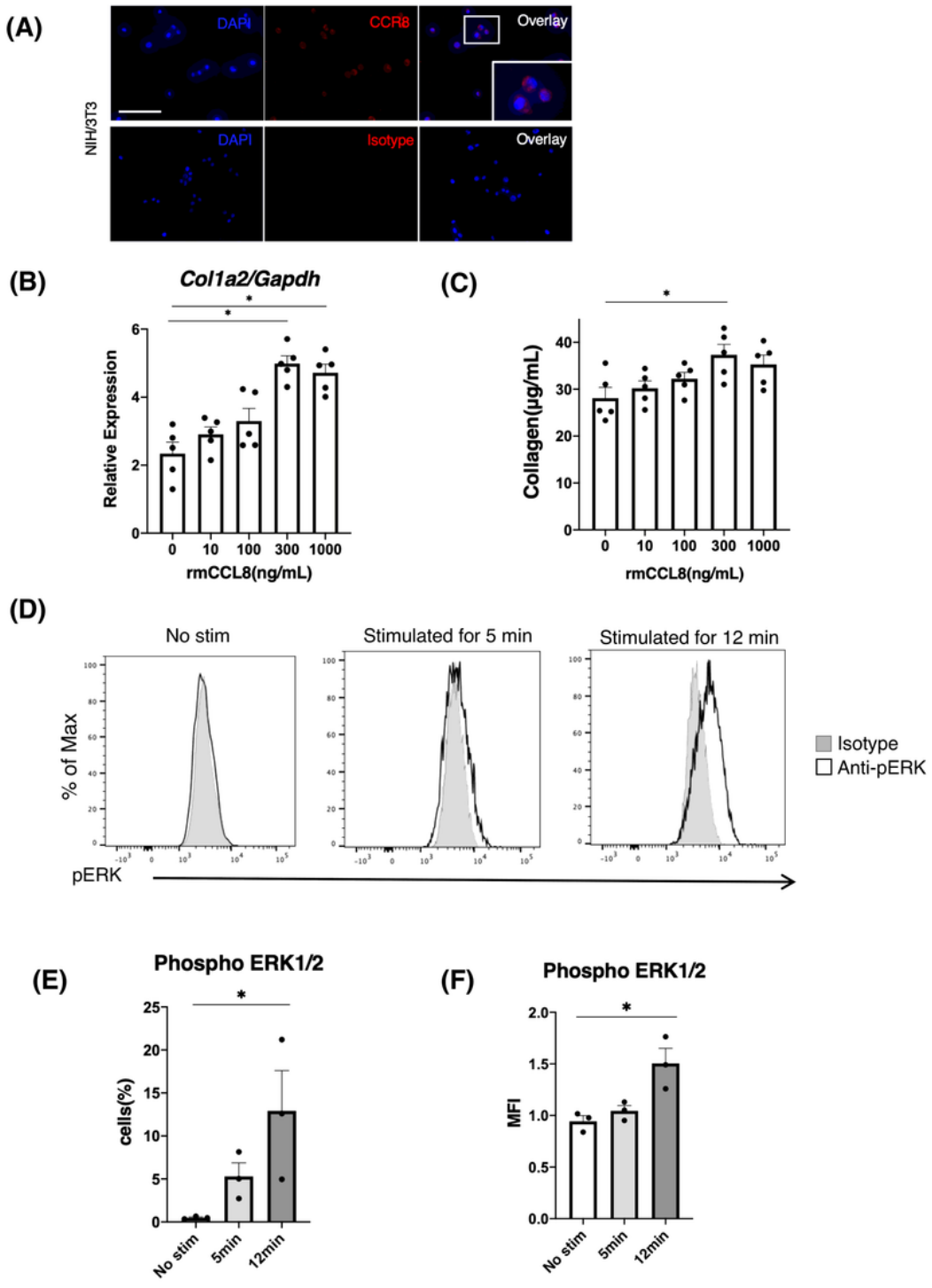

Figure 6

Effects of CCL8 on collagen production of fibroblasts in vitro (A) Immunofluorescence staining of CCR8 in a mouse fibroblast cell line (NIH/3T3). Upper panels: Alexa Fluor 546-conjugated anti-mouse CCR8 antibody staining. Lower panels: isotype control antibody staining. Original magnification ×40 (scale bar, 50 μm). DAPI, 4’6-diamino-2-phenylindole. (B) mRNA expression levels of Col1a2 in fibroblasts treated with recombinant mouse CCL8 for 24 h. (C) Total collagen protein production from fibroblasts treated

with recombinant mouse CCL8 for 24 h. (D) Flow cytometric analysis of phosphorylated ERK1/2 (pERK) in fibroblasts treated with recombinant mouse CCL8 at 300 ng/mL of concentration for the indicated times (min). The panels show a representative histogram of each of the 3 wells for the indicated times. (E) The bar graph shows the rate of pERK1/2-positive cells. (F) The bar graph shows the mean fluorescence intensity (MFI) of pERK1/2 in fibroblasts treated with recombinant mouse CCL8. The data are presented as means ± SEMs of 5 (B and C) and 3 (E and F) wells in each condition. *$p<0.05$, Kruskal-Wallis test.